



## Letter

# Three first order magnetic phase transitions in re-entrant ferromagnet $\text{PrMn}_{1.4}\text{Fe}_{0.6}\text{Ge}_2$

R. Zeng<sup>a,\*</sup>, J.L. Wang<sup>b,c</sup>, L. Lu<sup>a</sup>, W.X. Li<sup>a</sup>, S.J. Campbell<sup>b</sup>, S.X. Dou<sup>a</sup>

<sup>a</sup> Institute for Superconducting and Electronic Materials, University of Wollongong, Wollongong, NSW 2522, Australia

<sup>b</sup> School of Physical, Environmental and Mathematical Sciences, University of New South Wales, Australian Defense Force Academy, Canberra ACT 2600, Australia

<sup>c</sup> Bragg Institute, ANSTO, Lucas Heights, NSW 2234, Australia

## ARTICLE INFO

## Article history:

Received 15 March 2010

Received in revised form 11 June 2010

Accepted 12 June 2010

Available online 25 June 2010

## Keywords:

Magnetic phase transition

First order

Re-entrant magnet

## ABSTRACT

Three first order magnetic phase transitions (FOMTs) have been detected and evaluated over the temperature range from 5 to 340 K at fields up to 9 T in  $\text{PrMn}_{1.4}\text{Fe}_{0.6}\text{Ge}_2$ . All three FOMTs, from (with decreasing temperature) an antiferromagnetic (AFI) to a c-axis canted ferromagnetic (Fmc) state, to a c-axis canted antiferromagnetic (AFmc) state, and then to an Fmc state plus an additional Pr-sublattice magnetic contribution (Fmc + F(Pr)), exhibited temperature and field-induced transition features. A interesting phenomenon was observed, in that magnetic field can induce an AFmc to Fmc + F(Pr) transition, and then diminish and finally eliminate the re-entrant magnetic transition behavior under high field as well. Based on systematic measurements and analysis, a magnetic phase diagram has been determined.

Crown Copyright © 2010 Published by Elsevier B.V. All rights reserved.

## 1. Introduction

Ternary rare-earth (R) compounds of the type  $\text{RT}_2\text{X}_2$ , where T = transition metal, X = Si, Ge, exhibit a large variety of structural and physical properties and have been studied extensively over the years. The interesting phenomenon of re-entrant ferromagnetism has been found in several of these  $\text{RT}_2\text{X}_2$  compounds by controlling the interplay between the R–T and T–T exchange interactions through elemental substitution [1–3]. These are linked in part to their natural multilayer structure, which can exhibit either coupled magnetic and crystallographic transitions or valence-related transitions [e.g. refs. [4–8]]. It is well known that the main driving mechanism for the magnetism of the  $\text{RT}_2\text{X}_2$  type compounds is the strong dependence of Mn–Mn intraplanar and interplanar exchange interactions on  $d_{\text{Mn–Mn}}$ , the Mn–Mn separation distance in the *ab*-plane [2,9,10]. The magnetic structures and properties of  $\text{PrMn}_{2-x}\text{Fe}_x\text{Ge}_2$  have been studied recently over the entire Mn and Fe concentration ranges [1]. In this Letter, interest is focussed on the magnetic phase transition features of the re-entrant ferromagnet  $\text{PrMn}_{1.4}\text{Fe}_{0.6}\text{Ge}_2$  under variation of temperature and magnetic field. It has been found that two first order temperature and field-induced magnetic phase transitions, from a c-axis canted ferromagnetic (Fmc) state, to a c-axis canted antiferromagnetic (AFmc) state, and from the AFmc state to an Fmc state plus an additional magnetic contribution from the Pr-sublattice (Fmc + F(Pr)), merge together

with increasing magnetic field and finally vanish when the external field is raised to 9 T. A magnetic phase diagram was determined based on systematic magnetic measurements and analysis.

## 2. Experimental

Polycrystalline  $\text{PrMn}_{1.4}\text{Fe}_{0.6}\text{Ge}_2$  compound was prepared by arc melting the high purity elements on a water-cooled Cu hearth under purified argon gas. The mass loss of Mn during melting was compensated for by adding 2% excess Mn. The ingots were melted five times to attain homogeneity and then annealed at 900 °C for one week in an evacuated quartz tube. The room temperature X-ray diffraction pattern (Cu K $\alpha$  radiation) confirms the single-phase nature of the  $\text{PrMn}_{1.4}\text{Fe}_{0.6}\text{Ge}_2$  compound, which crystallizes in the  $\text{ThCr}_2\text{Si}_2$ -type structure with no evidence of any impurity phases. The X-ray data were refined using a Rietveld profile fit (FULL-PROF program), and the results of the refinements for the lattice parameters are  $a = 0.4088(1)$  nm and  $c = 1.0834(1)$  nm. The temperature dependence of the magnetization of  $\text{PrMn}_{1.4}\text{Fe}_{0.6}\text{Ge}_2$  was measured in magnetic fields of 0.01–9 T in both cooling and heating modes over the temperature range from 5 to 340 K. The experiments were carried out on a physical properties measurement system (PPMS) with a superconducting quantum interference device (SQUID).

## 3. Results and discussion

The temperature dependence of the  $\text{PrMn}_{1.4}\text{Fe}_{0.6}\text{Ge}_2$  magnetization on cooling and heating from 5 to 340 K in magnetic fields from 0.01 T to 9 T is presented in Fig. 1(a). As shown in Fig. 1(a), the temperature dependence of the magnetization for  $\text{PrMn}_{1.4}\text{Fe}_{0.6}\text{Ge}_2$  reveals the presence of four magnetic transitions, similar to the case of  $\text{SmMn}_2\text{Ge}_2$  [11–13]. Based on the magnetic structures of  $\text{PrMn}_2\text{Ge}_2$  [14,15] and the similarity in magnetic behavior of  $\text{PrMn}_{1.4}\text{Fe}_{0.6}\text{Ge}_2$  to that of  $\text{SmMn}_2\text{Ge}_2$ , it can be seen that with decreasing temperature from 340 K,  $\text{PrMn}_{1.4}\text{Fe}_{0.6}\text{Ge}_2$  exhibits a

\* Corresponding author.

E-mail address: [rzeng@uow.edu.au](mailto:rzeng@uow.edu.au) (R. Zeng).

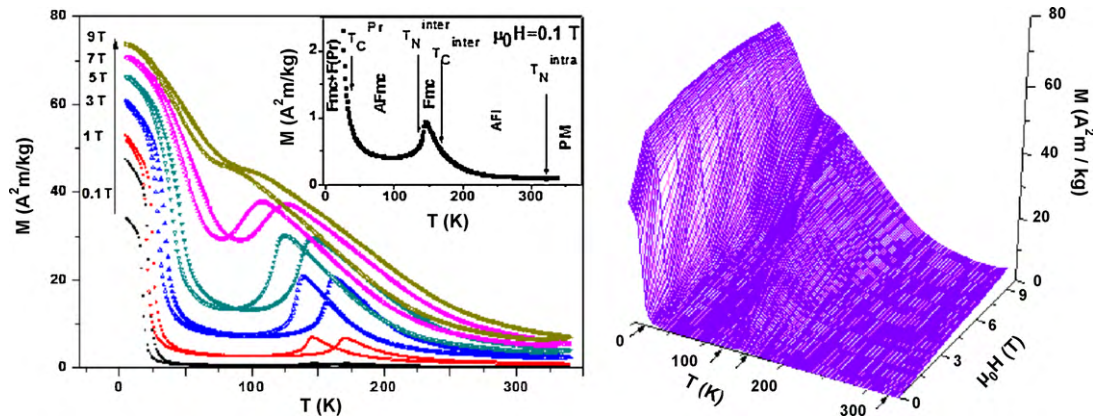


**Fig. 1.** (a) Temperature dependence of the magnetization for  $\text{PrMn}_{1.4}\text{Fe}_{0.6}\text{Ge}_2$  on cooling (open symbols) and heating (solid symbols) over the range of 5 to 340 K for magnetic fields from 0.01 T to 9 T, with the inset showing the magnetic transition temperatures for  $H = 0.1$  T; and (b) the  $M$ - $H$ - $T$  3D surface plots (cooling curves). For convenience the transition temperatures in zero field are indicated by arrows, cf. (a)).

transition from paramagnetism (PM) to an *ab*-plane antiferromagnetic state (AFI) [3] at the Néel temperature,  $T_N^{\text{intra}} \approx 333$  K. Around the Curie temperature,  $T_C^{\text{inter}} \approx 168$  K, this AFI structure gives way to a canted ferromagnetic structure of the Fmc type. With further decrease in temperature, a canted antiferromagnetic structure (AFmc) state occurs around  $T_N \approx 157$  K and, finally, there is a transition to an Fmc state plus an additional Pr-sublattice magnetic contribution (Fmc + F(Pr)) at  $T_C^{\text{Pr}} \approx 25.5$  K. Both  $\text{PrMn}_{1.4}\text{Fe}_{0.6}\text{Ge}_2$  and  $\text{SmMn}_2\text{Ge}_2$  exhibit similar magnetic behavior [3], even though the values of the room temperature *a*-parameters differ by  $\sim 1\%$  ( $a = 0.4088$  nm and  $a \approx 0.4045$  nm [12] respectively). This common magnetic behavior for disparate values of the *a*-parameter may be related to electronic effects, as suggested in the case of  $\text{NdMn}_{1.6}\text{Fe}_{0.4}\text{Ge}_2$ , for which the ferromagnetic to antiferromagnetic transition takes place at a larger  $d_{\text{Mn-Mn}}$  distance than in the pure  $\text{NdMn}_2\text{Ge}_2$  compound [11].

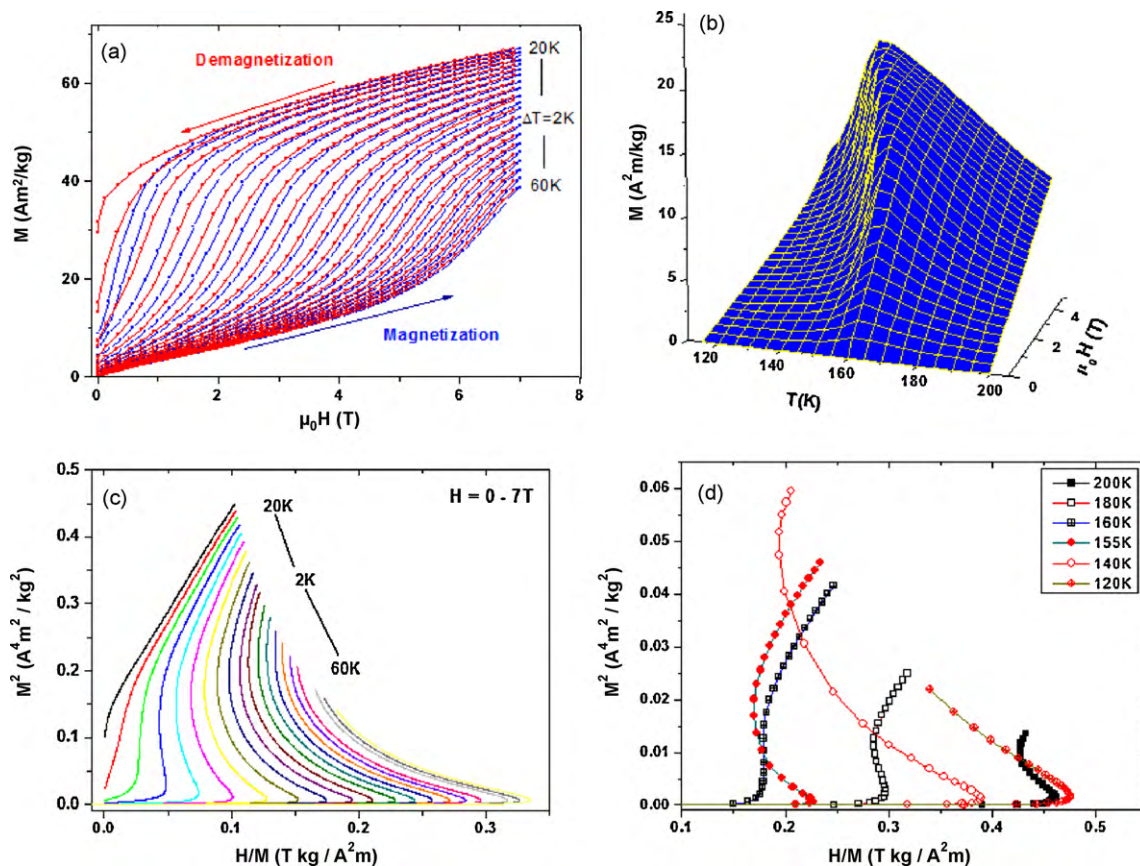
In order to further understand these magnetic transitions, the thermomagnetic curves at different applied fields are presented in Fig. 1(b) as 3D surface plots. These curves indicate clearly that the width of the lower temperature Fmc phase region increases with applied magnetic field, while the antiferromagnetic phase region decreases, thus demonstrating that the applied magnetic field destroys the AFmc state in  $\text{PrMn}_{1.4}\text{Fe}_{0.6}\text{Ge}_2$ . (This is also confirmed by the appearance of the field-induced metamagnetic phase transitions in the magnetization curves at 20 K and 60 K, as shown in Fig. 2(a).) It is well known that in  $\text{RMn}_2\text{Ge}_2$  compounds, even slight variations in the unit cell parameters due to external factors, such as pressure, field, temperature, or chemical substitution, are sufficient to modify the interlayer Mn–Mn spacing, leading to magnetic phase transitions [e.g. refs. [12,15]]. Such transitions are likely to be accompanied by an anomaly in the thermal expansion (magneto-volume effect) and can therefore be controlled by application of pressure or field. It has been reported that the width of the lower temperature antiferromagnetic phase in  $\text{SmMn}_2\text{Ge}_2$  can be extended by applied hydrostatic pressure [12]. By comparison, the present results demonstrate that an applied magnetic field on  $\text{PrMn}_{1.4}\text{Fe}_{0.6}\text{Ge}_2$  has the opposite effect to that of applied pressure on  $\text{SmMn}_2\text{Ge}_2$ ; this behavior can be understood in terms of magnetostriction, since magnetostriction effects generally induce tensile strain opposite to the pressure strain. It can also be seen from Fig. 1(b) that with increasing field, the gorge-like AFmc region between  $T_C^{\text{Pr}}$  and  $T_N^{\text{inter}}$  becomes narrow and shallow, and is almost closed above 9 T, which indicates that the “gorge” disappears and the re-entrant feature has vanished. The sharp cliff-like transition of AFmc to Fmc + F(Pr) at low field implies a large magnetocaloric effect, which will be confirmed in the future.

Fig. 2(a) shows the magnetization and demagnetization curves between 20 K and 60 K measured at 2 K intervals, with the  $M$ - $T$ - $H$  3D surface plots over the range of 100–200 K (5 K intervals) shown in Fig. 2(b). It is clear that above  $T_C^{\text{Pr}} \approx 25.5$  K and below  $T_N^{\text{inter}} \approx 157$  K, while the magnetization increases slowly with magnetic field in the low-field range before increasing sharply at a critical field, the magnetization is not saturated at 7 T between 25.5 K and 157 K. The steps in the magnetization curves indicate a field-induced feature of an antiferromagnetic (AFM) to ferromagnetic (FM) or FM to AFM phase transition. In order to determine the transition type, whether it is first or second order, the Inoue–Shimizu model, which involves a Landau expansion of the magnetic free energy up to the sixth power of the total magnetization  $M$ , has been used:

$$F(M, T) = \left( \frac{c_1(T)}{2} \right) M^2 + \left( \frac{c_2(T)}{4} \right) M^4 + \left( \frac{c_3(T)}{6} \right) M^6 + \dots - \mu_0 H M. \quad (1)$$

It has been reported [16] that the order of a magnetic transition is related to the sign of the Landau coefficient  $c_2(T)$ . A transition is expected to be first order when  $c_2(T_C)$  is negative, whereas it will be second order for a positive  $c_2(T_C)$ . The sign of  $c_2(T_C)$  can be determined by means of Arrott plots: if the Arrott plot is S-shaped near  $T_C$ , then  $c_2(T_C)$  is negative, otherwise,  $c_2(T_C)$  is positive. The Arrott plots of  $H/M$  versus  $M^2$  at 2 K intervals between 20 K and 60 K, and at selected temperatures between 120 K and 200 K are shown in Fig. 2(c) and (d), respectively. It can be seen that the magnetic transitions from AFI to Fmc above 168 K, from Fmc to AFmc below 157 K, and from AFmc to Fmc + F(Pr) below 25.5 K are first order transitions in applied magnetic field.

In order to precisely determine the critical temperature and boundary of the magnetic phase transitions, the  $dM/dT$  versus  $T$  curves are plotted in Fig. 3(a) and (b); and  $1/M$  versus  $T$  curves are plotted in Fig. 3(c) and (d). The cooling down ((a) and (c)), and the heating up ((b) and (d)) curves are both included, while the insets (in Fig. 3(a) and (b)) show the  $dM/dT$  -  $T$  curves at  $H = 0.1$  T with cooling down (a) and at  $H = 5$  T with heating up (b). The small vertical arrows indicate the positions of the minima in the derivative, from which the critical temperature values are determined. A field-induced metamagnetic phase transition from AFmc to Fmc + F(Pr) has been detected and analyzed above in Fig. 2(a); the transition is evident from the  $dM/dH$  versus  $H$  curve shown in Fig. 4(a). This suggests that the ferromagnetic ordering of  $\text{PrMn}_{1.4}\text{Fe}_{0.6}\text{Ge}_2$  can be shifted to higher temperatures by an applied magnetic field, or that the critical field ( $H_{\text{cr}}$ ) of a field-induced ferromagnetic ordering transition can be reduced by decreasing the temperature. The



**Fig. 2.** (a) Magnetization and demagnetization curves; (b)  $M$ – $T$ – $H$  3D surface plots at 5 K intervals between 100 and 200 K; (c) Arrott plots of  $H/M$  versus  $M^2$  at 2 K intervals between 20 and 60 K and (d) Arrott plots  $H/M$  versus  $M^2$  at the temperatures indicated.

temperature dependence of the critical magnetic field ( $H_{cr}$ ) of the metamagnetic transition around  $T_C^{Pr} = 25.5$  K is shown in the inset of Fig. 4(a). By using the same analysis method, the phase boundaries around the other two transition temperatures can be determined from the turning points of graphs of  $dM/dH$  versus  $H$  in

Fig. 4(b) for  $T_N^{inter} = 157$  K at 5 K intervals and (c) for  $T_C^{inter} = 168$  K at 5 K intervals. The insets show the temperature dependence of the critical field,  $H_{cr}$ , of the respective metamagnetic transition.

Based on systematic measurements and analysis, the magnetic phase diagram (magnetic field versus temperature) shown in Fig. 5

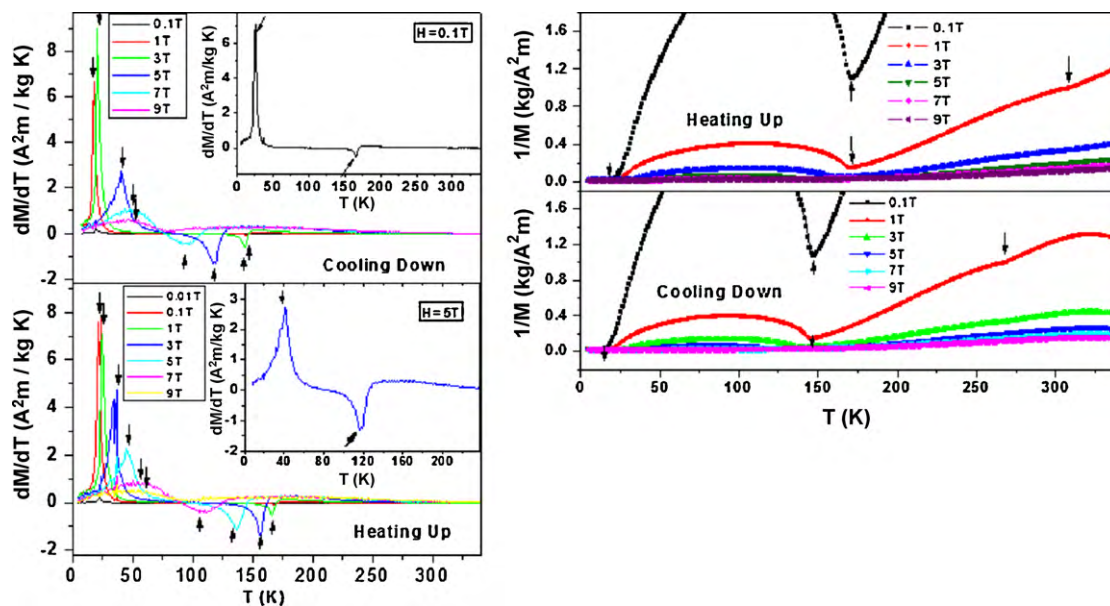


**Fig. 3.**  $dM/dT$  versus  $T$  curves over the range of 5 to 340 K for magnetic fields from 0.01 T to 9 T during cooling down (a) and during heating up (b), with the inset to (b) showing the  $dM/dT$  curve at  $H = 0.1$  T for cooling down, and the inset to (b) the  $dM/dT$  curve at  $H = 5$  T for heating up; and the  $1/M$  versus  $T$  curves with cooling down (c) and with heating up (d). The maxima and minima in the derivative are marked by arrows.



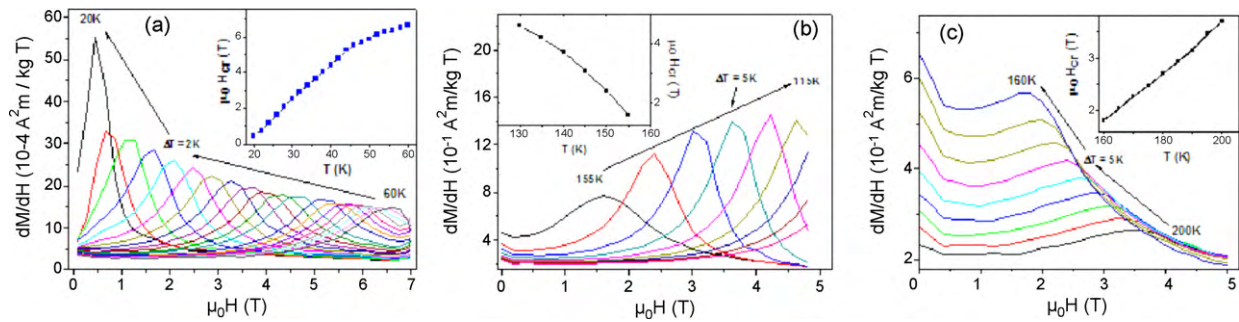


**Fig. 4.**  $dM/dH$  versus  $H$  curves around: (a)  $T_C^{\text{Pr}} = 25.5$  K at 2 K intervals; (b)  $T_N^{\text{inter}} = 157$  K at 5 K intervals; and (c)  $T_C^{\text{inter}} = 168$  K at 5 K intervals. The respective insets show the temperature dependence of the critical magnetic field ( $H_{\text{cr}}$ ) of the metamagnetic transition.

has been determined. The phase boundaries were determined from the  $dM/dT$  versus  $T$  and  $1/M$  versus  $T$  curves, as discussed in the text. This magnetic phase diagram for  $\text{PrMn}_{1.4}\text{Fe}_{0.6}\text{Ge}_2$  in Fig. 5 enables us to easily understand the unique magnetic behavior and magnetic phase transitions of this compound. As indicated in Fig. 5,  $T_N^{\text{inter}}$  decreases and  $T_C^{\text{Pr}}$  increases as the magnetic field increases, resulting in a narrowing of the canted AFmc antiferromagnetic range. The field dependences of these magnetic phase transition temperatures are derived to be:  $dT_C^{\text{inter}}/\mu_0 dH = 6.25$  K/T;  $dT_N^{\text{inter}}/\mu_0 dH = -8.3$  K/T, and  $dT_C^{\text{Pr}}/\mu_0 dH = 21.4$  K/T, with fitting results shown by the lines in Fig. 5. The same results can be obtained by line fitting the  $H_{\text{cr}}$  versus  $T$  curves in the insets of Fig. 4(a)–(c). The  $T_C^{\text{inter}}$  increases as the magnetic field increases. Similar behaviors have been found in other systems with re-entrant ferromagnetism, including  $\text{SmMn}_2\text{Ge}_2$  [17];  $\text{NdMn}_{1.575}\text{Fe}_{0.425}\text{Ge}_2$  (where  $dT_N^{\text{inter}}/\mu_0 dH = -13$  K/T and  $dT_C^{\text{Pr}}/\mu_0 dH = 8$  K/T) [12];  $\text{PrMn}_{0.6}\text{Fe}_{0.4}\text{Ge}_2$  [18]; and  $\text{Nd}_{0.35}\text{La}_{0.65}\text{Mn}_2\text{Si}_2$  [9]. It will be very interesting to know the magnetic state of the crossover point ( $T_C^{\text{Pr}} - \mu_0 H$  line and  $T_N^{\text{inter}} - \mu_0 H$  line) and the region higher than this point, which will be investigated in the future.

On the other hand, it has been reported that the antiferromagnetic range in  $\text{SmMn}_2\text{Ge}_2$  [19] becomes wider when hydrostatic pressure is applied ( $dT_C^{\text{R}}/\mu_0 dH = -91$  K/kbar and  $dT_N^{\text{inter}}/\mu_0 dH = -22.3$  K/kbar). This indicates that the influence of an applied magnetic field on the magnetic phase transitions is opposite to that from external pressure; this behavior can be understood in terms

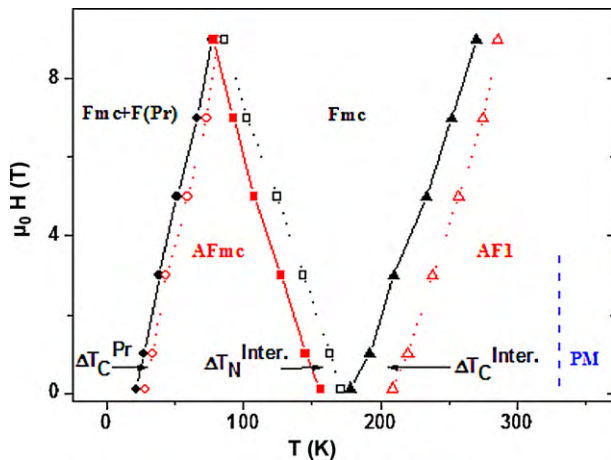


**Fig. 5.** Magnetic phase diagram of  $\text{PrMn}_{1.4}\text{Fe}_{0.6}\text{Ge}_2$  for applied magnetic fields in the range of 0–9 T and temperatures from 5 to 340 K. The PM, AF1, Fmc, AFmc, and Fmc+F(Pr) are defined as the paramagnetic, antiferromagnetic,  $c$ -axis ferromagnetic,  $c$ -axis antiferromagnetic, and  $c$ -axis ferromagnetic with added Pr ion ferromagnetic states, respectively; and  $\Delta T_C^{\text{Pr}}$ ,  $\Delta T_N^{\text{inter}}$ , and  $\Delta T_C^{\text{inter}}$  are defined as the thermal hysteresis temperature of the three phase transitions as described in the text.

of the spontaneous magneto-volume effect observed in these systems [9,18], as described above. The origin of this behavior may be the competition or balance between magnetostriction and pressure stress, since magnetostriction effects generally induce tensile strain in a direction opposite to that induced by pressure strain. It can also be seen from Fig. 5 that there is thermal hysteresis at  $\Delta T_C^{\text{Pr}} \approx 4.5$  K for the AFmc to Fmc + F(Pr) transition, at  $\Delta T_N^{\text{inter}} \approx 16$  K for the Fmc to AFmc transition, and at  $\Delta T_C^{\text{inter}} \approx 24$  K for the AF1 to Fmc transition, respectively. The thermal hysteresis also is a sign of a first order phase transition [20].

At high field ( $>9$  T), the re-entrant phenomenon will disappear due to the results of the competition of magnetostriction and pressure stress, which cancels out the magneto-volume effect induced AFM transition between Fmc and Fmc + F(Pr) that occurs at low field. The crystal volume shrinkage will be suppressed at high field. Only the transition between Fmc and Fmc + F(Pr) exists at higher fields, e.g., it is only due to the addition of the real or apparent Pr ferromagnetism, while the  $c$ -axis ferromagnetism (Fmc) of the Mn ions remains unchanged.

#### 4. Summary

Three magnetic phase transitions in  $\text{PrMn}_{1.4}\text{Fe}_{0.6}\text{Ge}_2$  over the temperature range from 5 to 340 K at fields up to 9 T: from the AF1 state to the Fmc state, from the Fmc state to the AFmc state, and from the AFmc to the Fmc + F(Pr) state (with an additional Pr magnetic contribution), were detected and identified to be FOMT. These three FOMTs were evaluated to exhibit temperature and field-induced transition features. An interesting phenomenon was observed, in that magnetic field can induce an antiferromagnetic to ferromagnetic transition and can diminish or eliminate the re-entrant magnetic transition behavior as well, as shown in Fig. 2(b), where the “gorge” disappears and the re-entrant feature vanishes when the field is higher than 9 T. A magnetic phase diagram with detected thermal hysteresis was determined over the measurement temperature and field range.

#### Acknowledgements

The authors thank Dr. T. Silver for her help and useful discussions. This work is supported by the Australian Research Council through a Discovery project (project ID: DP0879070).

#### References

- [1] R. Welter, B. Malaman, J. Alloys Compd. 354 (2003) 35.
- [2] G. Venturini, R. Welter, E. Ressouche, B. Malaman, J. Magn. Magn. Mater. 150 (1995) 197.
- [3] J.L. Wang, S.J. Campbell, J.M. Cadogan, O. Tegus, A.J. Studer, M. Hofmann, J. Phys. Condens. Matter 18 (2006) 189; I. Dincer, A. Elmali, Y. Elerman, H. Ehrenberg, H. Fuess, G. Andre, J. Alloys Compd. 416 (2006) 22.

- [4] T. Fujiwara, H. Fujii H, T. Shigeoka, Phys. Rev. B 63 (2001) 174440.
- [5] S. Chaudhary, M.K. Chattopadhyay, K.J. Singh, S.B. Roy, P. Chaddah, E.V. Sampathkumaran, Phys. Rev. B 66 (2002) 014424.
- [6] M. Hofmann, S.J. Campbell, A.V.J. Edge, Phys. Rev. B 69 (2004) 174432.
- [7] A.M. Bebb, J.W. Taylor, J.A. Duffy, Z.F. Banfield, M.J. Cooper, M.R. Lees, J.E. McCarthy, D.N. Timms, Phys. Rev. B 71 (2005) 024407.
- [8] E.G. Gerasimov, N.V. Mushnikov, T. Goto, Phys. Rev. B 72 (2005) 064446.
- [9] G. Venturini, B. Malaman, E. Ressouche, J. Alloys Compd. 240 (1996) 139.
- [10] J.S. Lord, P.C. Riedi, G.J. Tomka, Cz. Kapusta, K.H.J. Buschow, Phys. Rev. B 53 (1995) 283; H. Fujii, T. Okamoto, T. Shigeoka, N. Iwata, Solid State Commun. 53 (1985) 715.
- [11] M. Duraj, R. Duraj, A. Szytula, J. Magn. Magn. Mater. 82 (1989) 319.
- [12] A. Szytula, J. Leciejewicz, Handbook of Crystal Structures and Magnetic Properties of Rare Earth Intermetallics, CRC Press, Boca Raton, 1994; G.J. Tomka, C. Ritter, P.C. Riedi, Cz. Kapusta, W. Kocemba, Phys. Rev. B 58 (1998) 6330.
- [13] I. Nowik, Y. Levi, I. Felner, E.R. Bauminger, J. Magn. Magn. Mater. 147 (1995) 373.
- [14] R. Welter, G. Venturini, E. Ressouche, B. Malaman, J. Alloys Compd. 218 (1995) 204.
- [15] K. Koyama, S. Miura, H. Okada, T. Shigeoka, S. Fujieda, A. Fujita, K. Fukamichi, K. Watanabe, J. Alloys Compd. 408–412 (2006) 118.
- [16] J. Inoue, M. Shimizu, J. Phys. F: Met. Phys. 12 (1982) 1811; N.H. Duc, D.T.K. Anh, P.E. Brommer, Physica B 319 (2002) 1.
- [17] M. Duraj, R. Duraj, A. Szytula, Z. Tomkowicz, J. Magn. Magn. Mater. 73 (1988) 240.
- [18] J.L. Wang, A.J. Studer, S.J. Campbell, M. Hofmann, J.M. Cadogan, Physica B 385–386 (2006) 326.
- [19] P. Kumar, K.G. Suresh, A.K. Nigam, A. Magnus, A.A. Coelho, S. Gama, Phys. Rev. B 77 (2008) 224427.
- [20] H. Yamada, T. Goto, Phys. Rev. B 68 (2003) 184417.